Analytical and Bioanalytical Chemistry (2018) 410:7385–7394
https://doi.org/10.1007/s00216-018-1344-8

RESEARCH PAPER

Protamine-gold nanoclusters as peroxidase mimics and the selective enhancement of their activity by mercury ions for highly sensitive colorimetric assay of Hg(II)

Yan-Qin Huang[1] · Sha Fu[1] · Yong-Sheng Wang[1] · Jin-Hua Xue[1] · Xi-Lin Xiao[2] · Si-Han Chen[1] · Bin Zhou[1]

Received: 26 June 2018 / Revised: 1 August 2018 / Accepted: 28 August 2018 / Published online: 13 September 2018

Abstract

We certify that protamine-gold nanoclusters (PRT-AuNCs) synthesized by one-pot method exhibit peroxidase-like activity. The catalytic activity of PRT-AuNCs followed typical Michaelis–Menten kinetics and exhibited higher affinity to 3,3′,5,5′-tetramethylbenzidine (TMB) as the substrate compared to that of natural horseradish peroxidase. Meanwhile, we found that Hg(II) could dramatically and selectively enhance the peroxidase-like activity of PRT-AuNCs, and the enhanced mechanism by Hg(II) was demonstrated to be generation of the cationic Au species and the partly oxidized Au species ($Au^{\delta+}$) by Hg^{2+}–Au^0/Au^+ interaction. Based on this finding, quantitative determinations of Hg(II) via visual observation and absorption spectra were achieved. The proposed strategy displays high selectivity that arises from the strong aurophilic interaction of mercury towards gold. Moreover, the developed method is highly sensitive with a wide linear range and low detection limit of 1.16 nM. This strategy is not only helpful to develop effective nanomaterials-based artificial enzyme mimics but also irradiative to discover new applications of artificial mimic enzymes in bio-detection, medical diagnostics, and biotechnology.

Keywords Protamine-gold nanoclusters · Peroxidase-like activity · Partly oxidized Au species · Hg^{2+}–Au^0/Au^+ interaction Colorimetric sensing · Mercury

Introduction

In recent years, the biosensors based on enzymes have attracted increasing interests due to the high substrate specificity and catalytic activity of enzymes under mild conditions [1, 2]. However, the most practical applications of natural enzymes are limited owing to their intrinsic drawbacks of poor stability to environmental conditions, high cost, and rigorous storage requirements. Therefore, the development of artificial enzyme mimics is highly desirable. The rapid advances in nanotechnology provide excitingly new opportunities for developing enzyme mimics [3, 4]. So far, various nanomaterial-based enzyme mimics have become promising alternatives to natural enzyme and applied widely in biosensors, immunoassay, and other fields [5–8]. This new progress of nanomaterials has led to the discovery of metal nanoclusters which have gathered considerable attention. Noble metal nanoclusters possess distinct electronic structures and properties that are fundamentally different from those of larger nanoparticles [4]. In particular, gold nanoclusters as artificial enzymes have been used in biological detection owing to their low toxicity, good biocompatibility, and excellent catalytic activity. With the rapid development of metal nanoclusters, various kinds of templates such as proteins, peptides, amino acid, and DNA have been adopted to synthesize AuNCs and AgNCs. For example, Li's group prepared bimetallic Au/Ag NCs with DNA as a template, which were further adopted as a selective probe for detection of iodide ions [9]. Tao and co-workers prepared BSA-stabilized Au nanoclusters for detection of dopamine [10]. Liu and Guo team synthesized amino acid-functionalized AuNCs for colorimetric detection of copper ions and histidine [11], and so on. Nevertheless, no

Electronic supplementary material The online version of this article (https://doi.org/10.1007/s00216-018-1344-8) contains supplementary material, which is available to authorized users.

✉ Yong-Sheng Wang
yongsheng.w@tom.com

[1] College of Public Health, University of South China, West Changsheng Road 28#, Hengyang 421001, Hunan, China

[2] College of Chemistry and Chemical Engineering, University of South China, Hengyang 421001, Hunan, China

reports were found by utilizing protamines as template to synthesize Au nanoclusters for the detection of metal ions. Moreover, some of enzyme mimics possess relatively low catalytic activity. Researchers have devoted great efforts to enhance the enzyme-like activity of nanomaterials. For instance, fully dispersed Pt entities on AuNPs could remarkably increase the activity of gold for hydrogenation catalysis [12]. The surface modification of BSA-stabilized AuNCs was also reported to improve their peroxidase-like activity [13]. In addition, the peroxidase-like activity of gold nanoparticles was also stimulated by using heavy metal ions [14, 15]. These reports are illuminating to improve the catalytic activity of enzyme mimics.

Protamines are low-molecular-weight basic proteins which have high arginine content [16]. They are naturally occurring substances in animal sperms, purified by the mature testes of certain fishes such as salmon and herring. The role of protamines in sperm is to bind with DNA to assist in forming a compact structure, delivering the DNA to the nucleus of the egg after fertilization. They have been successfully employed for efficient delivery of DNA in transfection study of cells [16]. Additionally, the attachment of DNA to gold microparticles by protamines could enhance the resistance to temperature and protease degradation [17]. Also, they are known to exhibit cell penetrating activity [17]. These characteristics of protamines can be ideally used as a template for the preparation of metal nanoclusters.

Hg(II) ion is generally considered to be one of the most toxic heavy metal ions that can interact strongly with various enzymes such as glucose oxidase and horseradish peroxidase to block their active sites, leading to the inhibition of the activity of enzymes [15, 18]. Thus, the accumulation of mercury in the human body could result in a series of disease [18]. Therefore, the monitoring of Hg^{2+} in environment and biosample becomes an increasing demand. To date, many instrument-based methods have been reported for the determination of Hg^{2+}, such as HPLC-cold vapor atomic fluorescence [19], atomic absorption [20], ICP-MS [21], and fluorescence [22]. Compared with above methods, colorimetric sensing has attracted more attention owing to its simplicity and conveniences and can be easily monitored by the naked eyes [23, 24]. Especially, nanomaterial-based assays of Hg^{2+} were also reported. Zhu et al. found that Hg^{2+} can inhibit peroxidase mimetic activity of BSA-Au clusters and hence enable the assay of Hg^{2+} [25]. Tseng et al. also reported the detection of Hg^{2+} by the inhibition of the peroxidase-like activity of Pt-AuNPs [26], and so on. However, taking advantage of the protamine-gold nanoclusters (PRT-AuNCs) as peroxidase mimics and their activity being selectively enhanced by mercury ions for the colorimetric detection of Hg^{2+} has not been described to the best of our knowledge.

In this contribution, we for the first time employed protamine as both a reducing agent and a stabilizer to prepare Au nanoclusters (PRT-AuNCs) that could insure biocompatibility and enable controllable catalysis. Different from the reported literatures [25] and traditional feature of Hg^{2+} ions to enzymes, we found that Hg^{2+} ions could selectively stimulate the peroxidase mimetic activity of as-prepared PRT-AuNCs, enhancing their ability to catalyze the chromogenic reaction of 3,3′,5,5′-tetramethylbenzidine (TMB) and H_2O_2. Based on this finding, quantitative detections of Hg^{2+} via visual observation and UV-vis absorption were achieved. The proposed strategy displays high selectivity arising from the strong aurophilic interaction of Hg to Au. Additionally, the developed method is highly sensitive due to a little change in enzyme activity could cause a dramatic effect on chromogenic reaction. This strategy would be helpful to develop effective artificial enzyme mimics and facilitate their wide application in bio-detection, medical diagnostics, and biotechnology.

Experimental

Materials and chemicals

Protamine sulfate and $HAuCl_4 \cdot 4H_2O$ were obtained from Sinopharm Chemical Reagent Co., Ltd. (Shanghai, China). $HgCl_2$ and 3,3′,5,5′-tetramethylbenzidine dihydrochloride (TMB) were supplied by Sigma-Aldrich (St. Louis, MO, USA). The concentrations of $HgCl_2$ and TMB working solutions were all 5 mM. All other chemicals, such as H_2O_2 solution (30 wt% aqueous), o-phenylenediamine (OPD), 2,2′-azinobis(3-ethylbenzothiozoline)-6-sulfonate (ABTS), HOAc, NaOAc, and H_2SO_4 were acquired from Beijing Chemicals Reagent Company (Beijing, China). All reagents were of analytical grade, and ultra-pure water (18.2 MΩ cm) was used throughout this work.

Apparatus

All absorption spectra were obtained on a Shimadzu UV-2450 spectrophotometer (Kyoto, Japan). Circular dichroism (CD) spectra were recorded by a JASCO J-815 circular dichroism spectrometer. X-ray photoelectron spectroscopy (XPS) was acquired on a Thermo Scientific Escalab 250Xi X-ray photoelectron spectrometer (Waltham, UK). Transmission electron microscopy (TEM) images were finished on a FEI Tecnai G2 F20 S-TWIN Field emission transmission electron microscope (OR, USA). A pH meter (Sartorius AG, Germany) was utilized for pH adjustment.

Synthesis of PRT-AuNCs

All glasswares used in this work were thoroughly soaked with aqua regia and rinsed with copious amount of doubly distilled water, then oven-dried prior to use. PRT-AuNCs were prepared

by one-pot method. Briefly, 25 mL of 10 mM $HAuCl_4$ was mixed with an aqueous solution of 25 mL of 2.5 mg mL^{-1} protamine sulfate. The mixture was vigorously stirred for 2 min at 37 °C, followed by the addition of 2.5 mL of 1 M NaOH. The reaction was allowed to proceed under vigorous stirring for 12 h at 37 °C. The color of the solution changed from light yellow to yellowish brown. The obtained PRT-AuNC solution was kept at 4 °C in the dark for further use.

Measurement of the peroxidase-like activity of PRT-AuNCs

The peroxidase-like activity of the as-prepared PRT-AuNCs was tested by using TMB, ABTS, and OPD as a chromogenic substrate, respectively. In a typical experiment, 40 μL of the PRT-AuNC stock solution, 40 μL of 5 mM TMB/ABTS/OPD solution, 60 μL of 0.01 M H_2O_2, and 50 μL of 5 μM Hg^{2+} solution were added into 80 μL of 0.2 M acetate buffer of pH 5.5, followed by adding an appropriate amount of water to a volume of 500 μL. The mixture was incubated for 30 min at room temperature, and then transferred for UV–vis scanning. Meanwhile, the colorimetric responses were observed with the naked eyes and a photograph was taken.

Steady-state kinetic analysis

The steady-state kinetic experiments were performed in a NaOAc buffer (pH 5.5) including 40 μL of PRT-AuNCs and 50 μL of 5.00 μM Hg^{2+} by varying the concentrations of TMB as substrate at a fixed concentration of H_2O_2 and vice versa. The apparent kinetic parameters were calculated by using the Lineweaver–Burk equation: $1/\nu = (1/V_{max})\ (1 + K_m/c)$, where ν, V_{max}, c, and K_m were the initial velocity, the maximum reaction velocity, the concentration of the substrate, and the Michaelis–Menten constant, respectively.

Assay for Hg^{2+} by PRT-AuNCs as peroxidase mimics

Into a 2-mL EP tube, 40 μL of the PRT-AuNCs stock solution, 40 μL of 5 mM TMB, and 60 μL of 0.01 M H_2O_2 were added into 80 μL of 0.2 M acetate buffer (pH 5.5). Thereafter, different concentrations of Hg^{2+} were added, followed by adding an appropriate amount of water to a volume of 500 μL. After the mixture was incubated for 30 min at room temperature, the colorimetric responses were observed with the naked eyes and a photograph was taken. After that, 80 μL of 0.2 mol L^{-1} H_2SO_4 was used to stop the catalytic reaction. Then ultraviolet spectra were measured at λ_{max} 450 nm and represented as $\Delta A = A_1 - A_0$, where A_0 and A_1 were the absorbance of the system without and with Hg^{2+}, respectively.

Result and discussion

Characterization of as-prepared PRT-AuNCs

In this work, we successfully prepared PRT-AuNCs by one-pot method using protamine as both a stabilizer and a reducing agent. The aqueous solution of as-prepared PRT-AuNCs showed yellowish brown in color (Fig. 1A), and yellowish

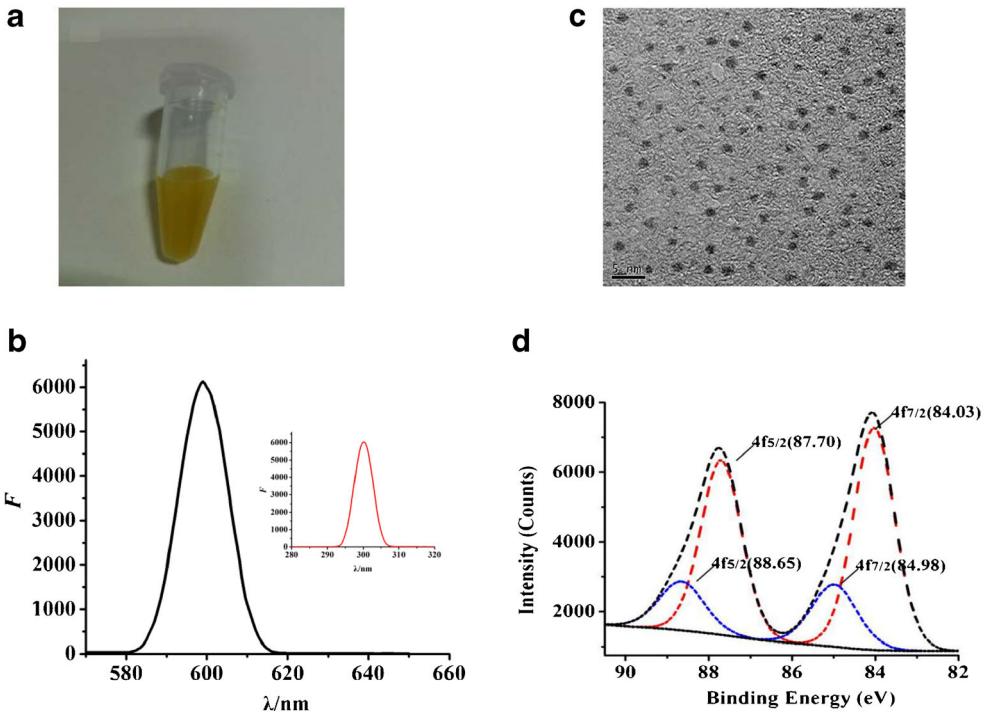

Fig. 1 **a** Visual observation of PRT-AuNCs under visible light, **b** emission and excitation (insert) spectra of PRT-AuNCs, **c** TEM image for PRT-AuNCs, and **d** XPS curves of Au^0 and Au^+ in the absence of Hg(II)

green fluorescence under 365 nm ultraviolet light (see the Electronic Supplementary Material (ESM), Fig. S1). Figure 1B indicates that the emission spectra of the PRT-AuNCs were about 599 nm upon excitation at 300 nm. To visualize the as-prepared PRT-AuNCs, a representative micrograph of the PRT-AuNCs was obtained by transmission electron microscopy (TEM) (Fig. 1C), which showed uniformly distributed particles. The average diameter of the PRT-AuNCs is less than 2 nm. Besides, X-ray photoelectron spectroscopy (XPS) showed that the binding energy of Au $4f_{7/2}$ and Au $4f_{5/2}$ for PRT-AuNCs was 84.1 eV and 88.0 eV, respectively (Fig. 1D). The Au $4f_{7/2}$ spectrum could be further deconvoluted into two distinct components centered at binding energies of 84.03 eV and 84.98 eV, which could be identified as Au^0 and Au^+, respectively. The integrated area of these two components demonstrates that the majority of gold in PRT-AuNCs is Au^0 with a minor amount of Au^+ at the surface of PRT-AuNCs. The presence of Au^+ in PRT-AuNCs might stabilize the AuNCs. The Au 4f XPS spectrum for PRT-AuNCs prompts that the Au^{3+} ions were reduced to Au^0 and Au^+ successfully by protamine. For the applications of as-prepared PRT-AuNCs, we carefully examined the stability of PRT-AuNCs. Interestingly, the aqueous solution of PRT-AuNCs as fluorescence probe was fairly stable even 1 month after preparation via tracking by fluorescence measurement (Fig. S2, see the ESM).

Peroxidase-like activity of as-prepared PRT-AuNCs

The peroxidase-like behavior of as-prepared PRT-AuNCs was examined by using TMB, ABTS, and OPD as chromogenic substrates, respectively. As shown in Fig. 2A, PRT-AuNCs could catalyze the fast oxidation of TMB, ABTS, and OPD in the presence of H_2O_2 and 0.50 μM Hg^{2+} to give different colors (Fig. 2A, insert), implying that PRT-AuNCs possess peroxidase-like activity. We further study the effect of dissolved oxygen on activity of PRT-AuNC enzyme mimics. Figure 2B shows that the absorbance of the system at 652 nm decreased obviously when the system was bubbled with N_2 for 2 h (curve b), and was further declined after saturation with N_2 for 5 h (curve c). This result indicated that the dissolved oxygen, which serves as an electron acceptor, played an important role in the oxidation of TMB.

To further investigate the catalytic mechanism of PRT-AuNCs as a peroxidase mimic, the steady-state kinetics method was adopted. The relationship between the initial reaction rate and the substrate concentration can commonly be described by the classic Michaelis–Menten model [27–30]. However, it is reported recently that the particular kinetic features for several CYP3A4 substrates cannot be explained within the context of the Michaelis–Menten model [31]. The PRT-AuNCs may be able to support multiple reactions simultaneously (i.e., multivalent interactions with substrate). So, the application of the classic

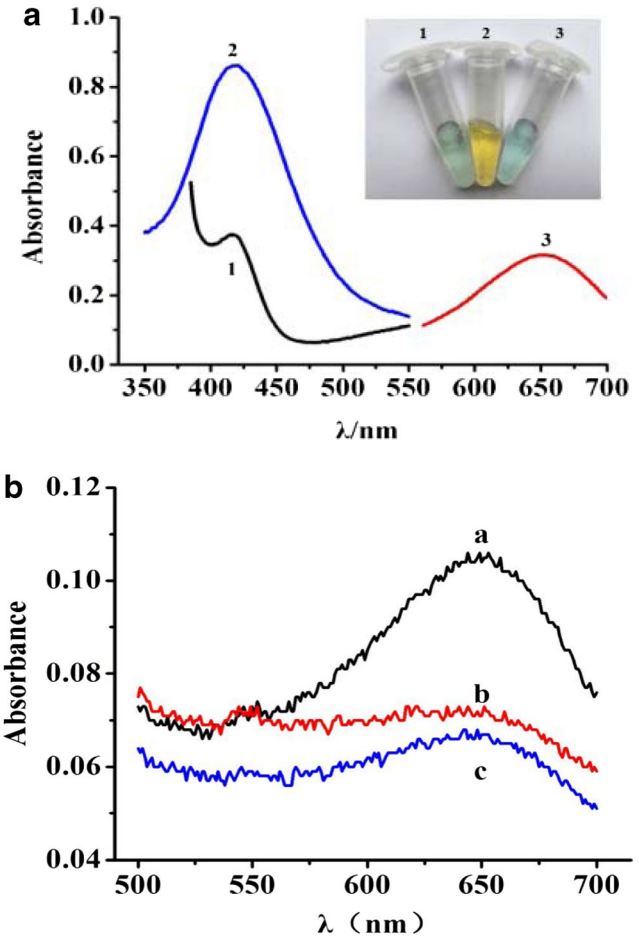

Fig. 2 **a** PRT-AuNCs catalyze the oxidation of various substrates to produce color reactions in the present of H_2O_2. (1) ABTS, (2) OPD, and (3) TMB. **b** Effect of O_2 concentration on the oxidation of TMB by PRT-AuNCs. (a) No N_2 was bubbled in NaOAc buffer. (b) The NaOAc buffer was bubbled with N_2 for 2 h. (c) The NaOAc buffer was bubbled with N_2 for 5 h. $V_{PRT\text{-}AuNCs} = 40$ μL, $c_{TMB} = 0.4$ mM, $c_{H2O2} = 1.2$ mM, $c_{Hg(II)} = 0.50$ μM

Michaelis–Menten model to describe the PRT-AuNCs catalysis may not be valid. To examine this supposition, the kinetic data were measured using H_2O_2 and TMB as substrates by implementing various concentrations of one substrate while keeping the other one constant. Figure 3A, B illustrates that in a certain range of substrate concentration, typical Michaelis–Menten curves were observed for PRT-AuNCs by using TMB and H_2O_2 as substrates. An apparent dependence relationship was obtained between the initial reaction rate and the substrate concentration. Figure 3C, D prompts that the reciprocal of the initial rate was directly proportional to the reciprocal of the substrate concentration, suggesting that the catalytic reaction of PRT-AuNCs followed the Michaelis–Menten behavior. The explanation of this result may be that there may be a smoothing over of any irregularities and the kinetics may look hyperbolic due to the "canceling out" of different kinetic features in the experimental condition [31]. The Michaelis–Menten constant (K_m) and maximum initial velocity (V_{max}) were obtained using the Lineweaver–

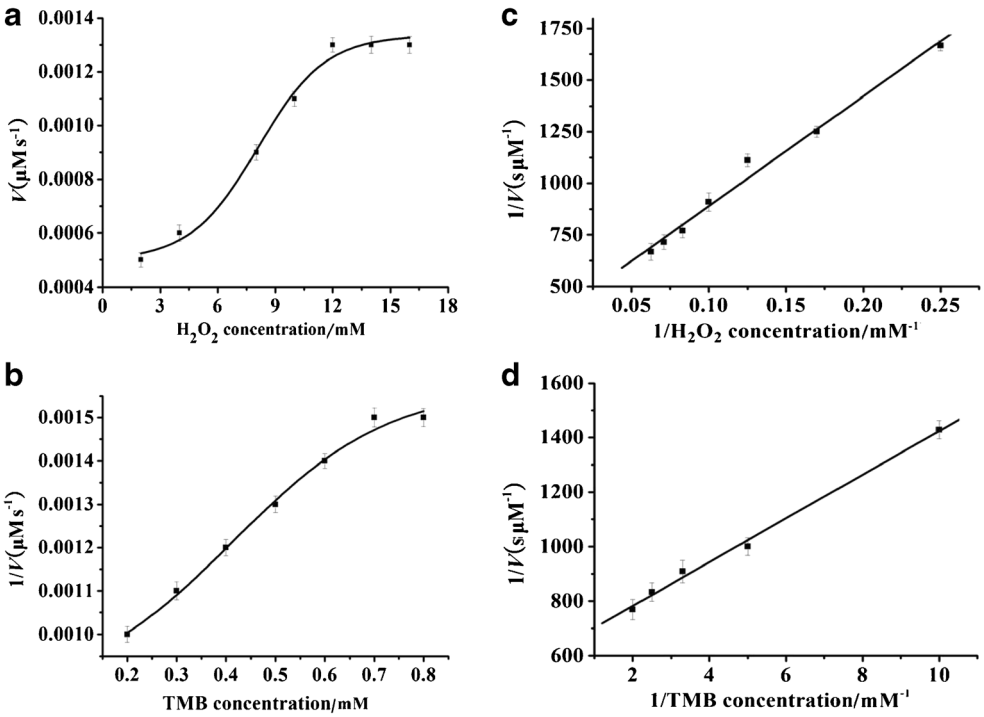

Fig. 3 Steady-state kinetic assay and catalytic mechanism of PRT-AuNCs. The velocity(v) of the reaction was measured using 40 μL of PRT-AuNCs and 50 μL of 5.00 μM Hg^{2+} in 80 μL NaOAc buffer (pH 5.5) at 25 °C. **a**, **c** The concentration of TMB was 0.4 mM and the H_2O_2 concentration varied. **b**, **d** The concentration of H_2O_2 was 1.2 mM and the TMB concentration varied. The error bars represent the standard deviations of three repetitive measurements

Burk plot, and the results are shown in Table 1. It is known that a lower K_m represents higher affinity to the substrate. From Table 1, the apparent K_m value of PRT-AuNCs (K_m = 0.169 mM) was much lower than that of horseradish peroxidase (HRP) (K_m = 0.434 mM) towards TMB [3], disclosing that PRT-AuNCs had a higher affinity for TMB than HRP. Meanwhile, the K_m value with H_2O_2 as substrate was 1.49 mM, which was about 2.5 times lower than that of HRP. This result was consistent with the observation that a lower H_2O_2 concentration was required for PRT-AuNCs when the maximum activity was obtained. Moreover, the PRT–AuNCs with TMB as substrate had a lower K_m value in comparison with other nanomaterial-based peroxidase mimics, such as CuNPs@C (K_m = 1.65 mM) [32], AgNCs ($K_m = 0.384 \pm 0.017$ mM) [33], MIL-101(Cr)@PB (K_m = 0.88 mM) [34], PBMNPs3 (K_m = 0.307 mM) [35], and GO–Fe_3O_4 (K_m = 0.43 mM) [36]. This result may ascribe to the fact that the PRT-AuNCs possess unique structure and properties that are fundamentally different from those of larger nanoparticles.

The catalytic activity of PRT-AuNCs also relies on pH and temperature variation. We examined the peroxidase-like activity of the PRT-AuNCs by changing pH from 3.5 to 7 and the temperature ranging from 10 °C to 45 °C. The optimal pH and temperature are pH 5.5 and 25 °C, respectively (ESM Figs. S3 and S4). This optimal temperature of 25 °C was considerably lower than that of native HRP (37 °C). Based on these results, a pH of 5.5 and temperature of 25 °C were employed as optimal conditions in subsequent experiments.

Table 1 Michaelis–Menten constant (K_m) and maximum initial velocity (V_{max})

Enzyme mimics	Substrate	K_m ($\times 10^{-3}$ mol L^{-1})	ν_{max} (mol L^{-1} s^{-1})
PRT-AuNCs	H_2O_2	1.49	2.80×10^{-6}
PRT-AuNCs	TMB	0.169	1.84×10^{-6}

Mechanism for the Hg(II)-enhanced peroxidase-like activity of PRT-AuNCs

The principle of the colorimetric sensing of Hg(II) is outlined in Scheme 1. It is reported that the slightly oxidized gold ($Au^{\delta+}$), in addition to metallic gold (Au^0) and Au^+, is important to achieve high activity of dispersed Au catalysts [25, 37–39]. Inspired by these reports, we hypothesized that the interaction of Hg^{2+} with Au^0/Au^+ on the surface of PRT-AuNCs might lead to the generation of the cationic Au species and the partly oxidized Au species ($Au^{\delta+}$). Such an $Au^{\delta+}$ and the cationic Au species as the peroxidase-like active sites of PRT-AuNCs might remarkably change their surface properties. Consequently, the peroxidase-like activity of the PRT-AuNCs was significantly enhanced by Hg(II), resulting in the change in the absorption intensity of the assay system. Thereby, a colorimetric detection system for Hg(II) could be developed.

To test this hypothesis, the interaction between PRT-AuNCs and Hg(II) was investigated using TMB as a chromogenic substrate by ultraviolet absorption spectra. Figure 2A indicates that PRT-AuNCs can catalyze the oxidation reaction of TMB by H_2O_2 to produce the typical blue color products (Fig. 2A, insert (3)). The maximum absorption peak of the system located at 652 nm, resulting from the oxidation of

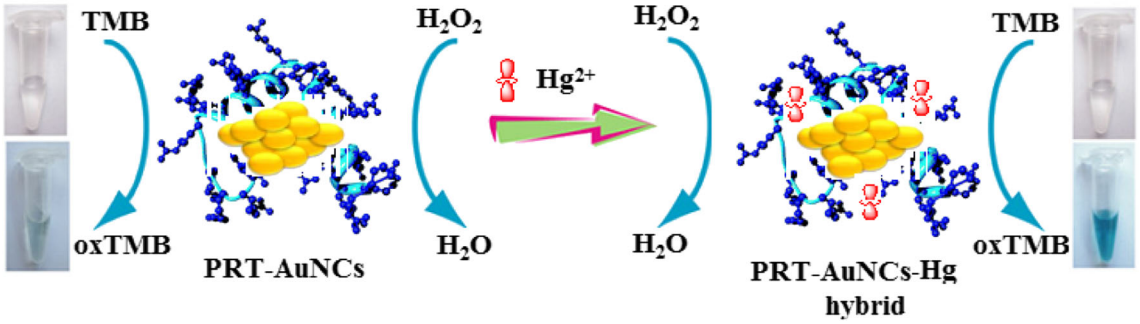

Scheme 1 The colorimetric detection of Hg(II) using PRT-AuNCs as peroxidase mimics and their activity being selectively enhanced by mercury ions

TMB. The addition of 80 μL of 0.2 mol L^{-1} H_2SO_4 in above-mentioned solution, a maximum absorption peak appeared at 450 nm (Fig. 4A, curve c). The control experiments showed that the absorbance of the PRT-AuNCs-TMB-H_2O_2-H_2SO_4 solution is much higher than that of TMB-H_2SO_4 and TMB-H_2O_2-H_2SO_4 system (Fig. 4A, curves a and b). This verified

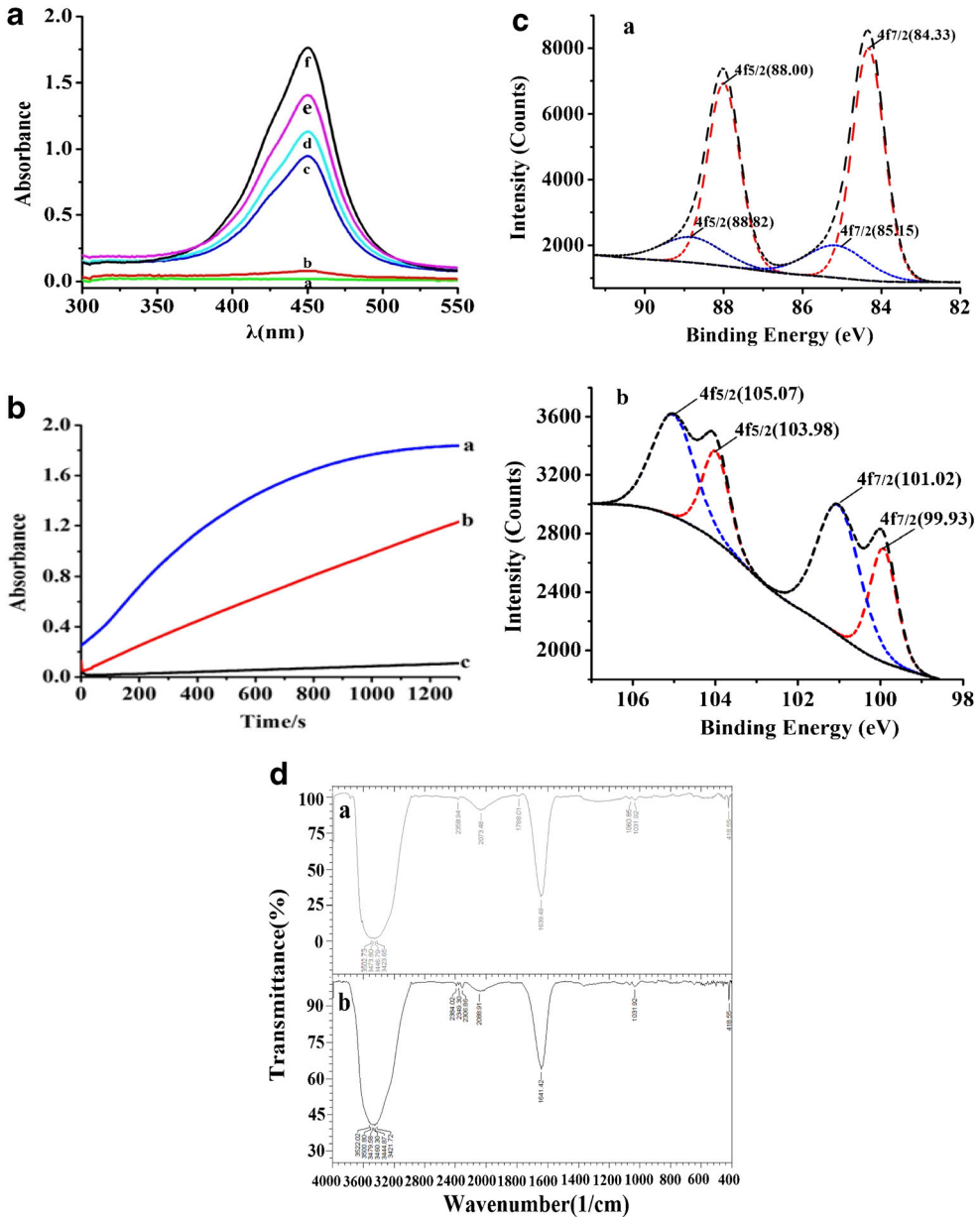

Fig. 4 **a** Enhancing effects of Hg(II) on the peroxidase-like activity of PRT-AuNCs. (a) TMB-H_2SO_4. (b) TMB-H_2O_2-H_2SO_4. (c) TMB-H_2O_2-PRT-AuNCs-H_2SO_4. (d–f) TMB-H_2O_2-PRT-AuNCs-Hg(II)-H_2SO_4 ($c_{Hg(II)}$ (10^{-7} M)/(d–f): 0.50, 5.0, 50.0). c_{TMB} = 0.4 mM, c_{H2O2} = 1.2 mM, $V_{PRT\text{-}AuNCs}$ = 40 μL. **b** Absorbance–time curves of PRT-AuNCs-Hg(II)-TMB-H_2O_2 (a), PRT-AuNCs-TMB-H_2O_2 (b), and TMB-H_2O_2 (c). $V_{PRT\text{-}AuNCs}$ = 40 μL, c_{TMB} = 0.40 mM, c_{H2O2} = 1.2 mM, $c_{Hg(II)}$ = 0.50 μM. **c** XPS curves of Au^0 and Au^+ in the presence of Hg(II) (a) and Hg^0 and Hg^{2+} in the presence of PRT-AuNCs (b). **d** FTIR spectra for (a) PRT-AuNCs and (b) PRT-AuNCs-Hg(II)

that the PRT-AuNCs are needed for the colorimetric reaction, which is similar to HRP. However, the addition of Hg(II) into the solution of PRT-AuNCs-TMB-H_2O_2-H_2SO_4 resulted in the gradually enhanced fluorescence signals (Fig. 4A, curves d–f), which was completely opposite to that reported by literatures [26]. This result indicates that Hg(II) could stimulate the peroxidase-like activity of PRT-AuNCs. The above-mentioned conclusion was also verified by the change of the real-time absorption intensity at 652 nm in the PRT-AuNCs-TMB-H_2O_2-Hg(II) system. As illustrated in curve c of Fig. 4B, the solution of TMB + H_2O_2 without PRT-AuNCs showed negligible absorption variations. Upon addition of PRT-AuNCs into this solution (curve b), the absorbances of the solution went up obviously ranging from 0 to 20 min, indicating that the PRT-AuNCs can catalyze the oxidation of TMB by H_2O_2 in a relatively slow reaction rate. Interestingly, a rapid increase of the reaction rate was observed with addition of Hg(II) in the above solution (curve a). This result indicated that Hg(II) can accelerate the PRT-AuNC-mediated oxidation of TMB in the presence of H_2O_2.

To validate whether the interaction of Hg^{2+} with Au^0/Au^+ could generate the cationic Au species and $Au^{\delta+}$, X-ray photoelectron spectroscopy (XPS) was obtained. Figure 4C (a) shows that the addition of Hg^{2+} into the PRT-AuNC solution caused an increase in the oxidation states of Au^0/Au^+ on the PRT-AuNCs in comparison with Fig. 1D. The binding energy changed from 84.98 to 85.15 eV corresponding to Au^+. An Au $4f_{7/2}$ peak of 84.33 eV appeared between 84.0 (Au^0) and 85.0 eV (Au^+), which is assigned to partly oxidized ionic Au species ($Au^{\delta+}$) [39]. Figure 4C (b) demonstrates that both Hg^0 and Hg^{2+} existed on the surface of PRT-AuNCs when they were incubated with Hg^{2+}. These results demonstrated our presumption. The above-mentioned conclusion was also confirmed by Fourier-transform infrared (FTIR) spectra. The protamine displayed an O–H/N–H stretching peak centered at 3473 cm^{-1}. While the C=O stretching vibrations (approximately 80%) coupled with in-plane N–H bending (approximately 20%) centered at 1640 cm^{-1} are attributed to amide I region, and a C–N stretching peak at 1061 cm^{-1} is assigned to aliphatic amine such as arginine residue in protamine (ESM Fig. S5) [40, 41], and no peaks in both amide II and amide III regions were found. The band around 2100 cm^{-1} may be caused by the asymmetric stretching vibrations of the $^+N–H\cdots O^-$ bond [42]. In comparison with protamine, the FTIR spectra of PRT-AuNCs revealed an apparent broadening O–H/N–H stretching vibration and an enhancing peak of C=O stretching coupled with in-plane N–H bending, accompanied by some new peaks located at 2359 cm^{-1}, 1788 cm^{-1}, and 1032 cm^{-1} (Fig. 4D (a)). Meanwhile, the asymmetric stretching of the $^+N–H\cdots O^-$ bond shifted for about 8 cm^{-1}. These results suggest that Au^0/Au^+ on the AuNCs might bind to the N atoms in amide I regions or the guanidyl group of arginine residues to form Au–N bond by coordinating interaction. The formation of Au–N coordinative bond might facilitate the oxidation of Au^0/Au^+ on the PRT-AuNCs surfaces in the presence of Hg^{2+}, which was consistent with the observation of XPS spectra. When Hg^{2+} was added in the solution of PRT-AuNCs, the significant decreases of the percent transmittances for the principal peaks like O–H/N–H and C=O were observed (Fig. 4D (b)), accompanied by the broadening of peak width for O–H/N–H, the disappearance of the peak at 1788 cm^{-1} and the change of the asymmetric stretching vibrations of the $^+N–H\cdots O^-$ bond. Furthermore, the some small peaks appeared at 2307–2384 cm^{-1}. These results suggest that the existences of the interactions of mercury ions with both Au^0/Au^+ and protamine, leading to the change of the coordination bond of Au^0/Au^+ with O–H/N–H and C=O/N–H in PRT-AuNCs. Also, the attachment of Hg^{2+} onto the surface of the protamine by coordination may facilitate Hg^{2+} to be close to the surface of AuNCs, promoting the interaction between Au^0/Au^+ with Hg^{2+} to improve the surface properties of the PRT-AuNCs.

Based on the above-mentioned experimental results and the clues from the literatures [15, 25, 40, 43], we could conclude that the specific enhancement of the peroxidase-like activity of the PRT-AuNCs by Hg^{2+} might involve in two steps. Firstly, Au^0/Au^+ that bind to protamine by Au–N bond can easily interact with Hg^{2+} to lead to the generation of the cationic Au species and the partly oxidized ionic Au species ($Au^{\delta+}$) on AuNC surface. Next, such an $Au^{\delta+}$ and Au^+ as the peroxidase-like active sites of PRT-AuNCs remarkably change the surface properties of the PRT-AuNCs, thereby significantly enhancing their peroxidase-like activity.

Optimization of the sensing conditions

To achieve a better sensing performance, several factors including the concentrations of PRT-AuNCs, TMB, H_2O_2, and reaction time were investigated. First, the influence of the amount of PRT-AuNCs on the sensing system was studied. Figure S6 (see the ESM) displays a maximum ΔF value upon the addition of 40–45 μL of PRT-AuNC solution. Thereby, 40 μL of PRT-AuNC solution was selected in this assay.

To evaluate the peroxidase-like activity of our designed PRT-AuNCs, we selected TMB as a chromogenic substrate in the presence of H_2O_2. So, TMB concentration was also optimized. Figure S7 (see the ESM) illustrates that the addition of 40 μL of 5 mM TMB can be oxidized completely by H_2O_2. While the gradual decrease of the absorbance was observed upon adding TMB beyond 50 μL. The reason may be that the excess TMB might result in incomplete oxidation by H_2O_2. Thus, 40 μL of 5 mM TMB was chosen. Figure S8 (see the ESM) shows when 10 to 60 μL of 0.01 M H_2O_2 was added, ΔA values went up quickly, then it declined in the added volumes ranging from 80 to 100 μL. The likely explanation is that the shortage of H_2O_2 could not oxidize TMB

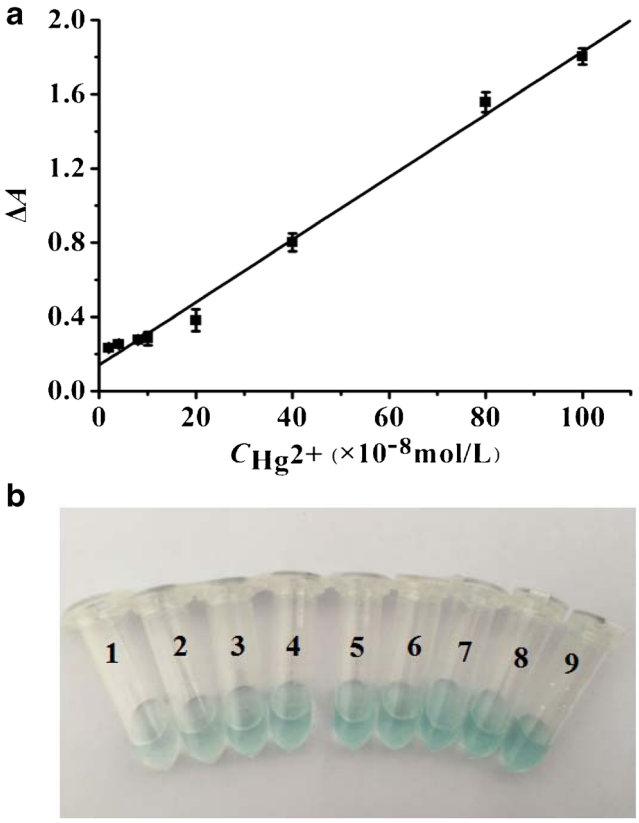

Fig. 5 Calibration curves (**a**) and visual observation (**b**) for colorimetric sensing of Hg(II). $V_{PRT\text{-}AuNCs} = 40$ μL, $c_{TMB} = 0.40$ mM, $c_{H2O2} = 1.2$ mM. **a** The error bars represent the standard deviations of three repetitive measurements. **b** $c_{Hg(II)}$ (10^{-8} M)/(1–9): 0.0, 2.0, 4.0, 8.0, 10.0, 20.0, 40.0, 80.0, 100.0

completely, suggesting that an appropriate amount of H_2O_2 is necessary for colorimetric detection of Hg^{2+}. Therefore, 60 μL of 0.01 M H_2O_2 was selected in the experiment. Figure S9 (see the ESM) displays that the ΔF initially increased rapidly with increasing reaction time and then tended to level off at 30 min. Thus, the reaction time of 30 min was selected in this study.

Selectivity and sensitivity of the sensing system

To evaluate the selectivity of the method, other substances were utilized in the assay based on the likely interference compositions. The results displayed that 1000 times of Ca^{2+} and Mg^{2+}; 100 times of K^+, Fe^{3+}, Zn^{2+}, Na^+, UO_2^{2+}, Mn^{2+}, NH_4^+, Cu^{2+}, Cd^{2+}, and Al^{3+}; 90 times of Ag^+; and 5 times of Pb^{2+} do not interfere with detection of Hg^{2+} (Fig. S10, see the ESM). Therefore, the method exhibits very good selectivity.

To validate the feasibility of this strategy, the calibration graph was described under the optimum conditions. A good linear correlation was observed within the concentration range of 4.0 nM–1.0 μM (Fig. 5A). The equations of linear regression are $\Delta A = 0.143 + 0.017c$ (10^{-8} mol L^{-1}) with the correlation coefficients of 0.9910. Based on an equation of LOD = $3S_b$/slope (S_b represents the standard deviation of the 11 blank measurements), the detection limit of 1.16 nM was obtained, which was 3–148 times lower than those of the colorimetric methods including the use of some enzyme mimics [25, 44–46], 2–5 times for fluorescence detection [47, 48], and 5–13 times for the other methods [18, 49]. Additionally, the linear range of this strategy is wider than that of the other methods as well (Table 2), which promotes the application of this method to determine Hg^{2+} in various types of samples. As shown in Fig. 5B, with increasing concentration of analyte, the color of the solution changed from light blue to deep blue gradually (here, H_2SO_4 was not added due to blue color giving more distinguished visual feeling). The color varied obviously and sensitively, which offered the possibility of visual observation for Hg^{2+} detection.

Table 2 Comparison of this strategy with other methods for the determination of Hg(II)

Methods	Analyte	Linearity ranges (nM)	LOD (nM)	Signal probe	Refs.
Flu	Hg^{2+}	10–400	2.5	Dye-labeled oligonucleotide	[47]
Flu	Hg^{2+}	10–5000	5	MSO-ThT	[48]
Col	Hg^{2+}	10–10,000	3	BSA-Au clusters	[25]
Col	Hg^{2+}	50–500 2000–7500	47	G-quadruplex DNAzyme	[44]
Col	Hg^{2+}	5–400	19	G-quadruplex DNAzyme	[45]
Col	Hg^{2+}	100–1000	148	T-S-AuNPs	[46]
RLS	Hg^{2+}	25–250	13	AuNPs-S	[18]
ECL	Hg^{2+}	5–250	5	TBR-Probe	[49]
This method	Hg^{2+}	4–1000	1.16	PRT-AuNCs	This work

Flu fluorometry, *MSO-ThT* mercury-specific oligonucleotide-thioflavin T, *Col* colorimetry, *T-S-AuNPs* thymine acetamido-ethanethiol (T-SH) on gold nanoparticles, *RLS* resonance light scattering, *AuNPs-S* sulfur ion (S^{2-})-modified gold nanoparticles, *ECL* electrochemi-luminescence, *TBR-Probe* tris (2,2-bipyridine) ruthenium (II)–probe

Table 3 Determination results of mercury ions in water samples ($n = 6$)

Sample	Found 10^{-7} mol L^{-1}	Added 10^{-7} mol L^{-1}	Total found 10^{-7} mol L^{-1}	Recovery (%)
1	–	4.00	4.112	102.9
2	–	4.00	3.992	99.81
3[a]	–	4.00	4.044	101.1
3[b]	–	4.00	4.006	100.2
3[c]	–	4.00	4.078	101.2

1 laboratory tap water, *2* pond water from the University of South China, *3*[a] Xiangjiang River water, *3*[b] Xiangjiang River water, *3*[c] Xiangjiang River water

Analysis of Hg^{2+} in real samples

To test the potential of the developed method for Hg^{2+} analysis, five water samples were collected from the pond water in the University of South China, Xiangjiang River, and tap water. All samples were filtered twice with quantitative filter paper, heating to boil for 10 min. After cooling to room temperature, the solutions were filtrated by 0.22 μm filter membrane. Then these samples were determined by the developed strategy. Recovery test was performed by the addition of a known amount of Hg^{2+} ions into samples, and the results are recorded in Table 3. It is obvious that the established method could be applied for Hg^{2+} assay in environmental samples.

Conclusions

In summary, we for the first time employed protamines as both a stabilizer and a reducing agent to synthesize gold nanoclusters in a mild condition. PRT-AuNCs were characterized using UV-vis, fluorescence, TEM, XPS, and FTIR, showing an efficient peroxidase-like activity. The catalytic activity of PRT-AuNCs followed typical Michaelis–Menten kinetics, exhibiting higher affinity to TMB as a substrate compared to that of natural HRP. Hg(II) can stimulate the peroxidase-like activity of PRT-AuNCs selectively and sensitively, which enables a label-free colorimetric assay of Hg(II) with a wide linear range and low detection limit of 1.16 nM. Furthermore, the mechanism for Hg(II)-enhanced peroxidase-like activity of PRT-AuNCs was investigated, finding that the interaction of Hg^{2+} with Au^0/Au^+ on AuNCs surface could generate the cationic Au species and the partly oxidized Au species ($Au^{\delta+}$). The proposed strategy may be helpful to develop new applications for AuNCs in varieties of simple, cost-effective, and easy-to-make sensors in biotechnology, medicine, and environmental chemistry.

Acknowledgements The authors gratefully acknowledge the support of the National Natural Science Foundation of China (No. 21177052, 81502850), the Natural Science Foundation of Hunan Province in China (No. 2015JJ2122), and the Science and Technology Program of Hunan Province in China (No. 2010SK3039).

Compliance with ethical standards

Conflict of interest The authors declare that they have no competing interests.

References

1. Jiang X, Sun C, Guo Y, Nie G, Xu L. Peroxidase-like activity of apoferritin paired gold clusters for glucose detection. Biosens Bioelectron. 2015;64:165–70.
2. Kwon D, Lee S, Ahn MM, Kang IS, Park KH, Jeon S. Colorimetric detection of pathogenic bacteria using platinum-coated magnetic nanoparticle clusters and magnetophoretic chromatography. Anal Chim Acta. 2015;883:61–6.
3. Wang Q, Zhang L, Shang C, Zhang Z, Dong S. Triple-enzyme mimetic activity of nickel-palladium hollow nanoparticles and their application in colorimetric biosensing of glucose. Chem Commun (Camb). 2016;52:5410–3.
4. Wei H, Wang E. Nanomaterials with enzyme-like characteristics (nanozymes): next-generation artificial enzymes. Chem Soc Rev. 2013;42:6060–93.
5. Li K, Wang K, Qin W, Deng S, Li D, Shi J, et al. DNA-directed assembly of gold nanohalo for quantitative plasmonic imaging of single-particle catalysis. J Am Chem Soc. 2015;137:4292–5.
6. Liu B, Sun Z, Huang JPJ, Liu J. Hydrogen peroxide displacing DNA from nanoceria: mechanism and detection of glucose in serum. J Am Chem Soc. 2015;137:1290–5.
7. Fan K, Xi J, Fan L, Wang P, Zhu C, Tang Y, et al. In vivo guiding nitrogen-doped carbon nanozyme for tumor catalytic therapy. Nat Commun. 2018; https://doi.org/10.1038/s41467-018-03903-8.
8. Lu C, Liu X, Li Y, Yu F, Tang L, Hu Y, et al. Multifunctional Janus hematite–silica nanoparticles: mimicking peroxidase-like activity and sensitive colorimetric detection of glucose. ACS Appl Mater Interfaces. 2015;7:15395–402.
9. Li Z, Liu R, Xing G, Wang T, Liu S. A novel fluorometric and colorimetric sensor for iodide determination using DNA-templated gold/silver nanoclusters. Biosens Bioelectron. 2017;96:44–8.
10. Tao Y, Lin Y, Ren J, Qu X. A dual fluorometric and colorimetric sensor for dopamine based on BSA-stabilized Au nanoclusters. Biosens Bioelectron. 2013;42:41–6.
11. Liu Y, Ding D, Zhen Y, Guo R. Amino acid-mediated 'turn-off/turn-on' nanozyme activity of gold nanoclusters for sensitive and selective detection of copper ions and histidine. Biosens Bioelectron. 2017;92:140–6.
12. Hong YC, Sun KQ, Zhang GR, Zhong RY, Xu BQ. Fully dispersed Pt entities on nano-Au dramatically enhance the activity of gold for chemoselective hydrogenation catalysis. Chem Commun (Camb). 2011;47:1300–2.
13. Han L, Li Y, Fan A. Improvement of mimetic peroxidase activity of gold nanoclusters on the luminol chemiluminescence reaction by surface modification with ethanediamine. Luminescence. 2018; https://doi.org/10.1002/bio.3472.
14. Lien CW, Chen YC, Chang HT, Huang CC. Logical regulation of the enzyme-like activity of gold nanoparticles by using heavy metal ions. Nanoscale. 2013;5:8227–34.
15. Long YJ, Li YF, Liu Y, Zheng JJ, Tang J, Huang CZ. Visual observation of the mercury-stimulated peroxidase mimetic activity of gold nanoparticles. Chem Commun (Camb). 2011;47:11939–41.

16. Sivamani E, DeLong RK, Qu R. Protamine-mediated DNA coating remarkably improves bombardment transformation efficiency in plant cells. Plant Cell Rep. 2009;28:213–21.
17. DeLong RK, Akhtar U, Sallee M, Parker B, Barber S, Zhang J, et al. Characterization and performance of nucleic acid nanoparticles combined with protamine and gold. Biomaterials. 2009;30:6451–9.
18. Fan Y, Long YF, Li YF. A sensitive resonance light scattering spectrometry of trace Hg^{2+} with sulfur ion modified gold nanoparticles. Anal Chim Acta. 2009;653:207–11.
19. Ramalhosaa E, Rıo Segadeb S, Pereira E, Valed C, Duartec A. Simple methodology for methylmercury and inorganic mercury determinations by high-performance liquid chromatography–cold vapour atomic fluorescence spectrometry. Anal Chim Acta. 2001;448:135–43.
20. de Jesus RM, Silva LOB, Castro JT, de Azevedo Neto AD, de Jesus RM, Ferreira SLC. Determination of mercury in phosphate fertilizers by cold vapor atomic absorption spectrometry. Talanta. 2013;106:293–7.
21. Wang M, Feng W, Shi J, Zhang F, Wang B, Zhu M, et al. Development of a mild mercaptoethanol extraction method for determination of mercury species in biological samples by HPLC-ICP-MS. Talanta. 2007;71:2034–9.
22. Chen SH, Wang YS, Chen YS, Tang X, Cao JX, Li MH, et al. Dual-channel detection of metallothioneins and mercury based on a mercury-mediated aptamer beacon using thymidine-mercury-thymidine complex as a quencher. Spectrochim Acta A Mol Biomol Spectrosc. 2015;151:315–21.
23. Tang X, Wang YS, Xue JH, Zhou B, Cao JX, Chen SH, et al. A novel strategy for dual-channel detection of metallothioneins and mercury based on the conformational switching of functional chimera aptamer. J Pharm Biomed Anal. 2015;107:258–64.
24. Wang Q, Yang X, Yang X, Liu P, Wang K, Huang J, et al. Colorimetric detection of mercury ion based on unmodified gold nanoparticles and target-triggered hybridization chain reaction amplification. Spectrochim Acta A Mol Biomol Spectrosc. 2015;136:283–7.
25. Zhu R, Zhou Y, Wang XL, Liang LP, Long YJ, Wang QL, et al. Detection of Hg^{2+} based on the selective inhibition of peroxidase mimetic activity of BSA-Au clusters. Talanta. 2013;117:127–32.
26. Tseng CW, Chang HY, Chang JY, Huang CC. Detection of mercury ions based on mercury-induced switching of enzyme-like activity of platinum/gold nanoparticles. Nanoscale. 2012;4:6823–30.
27. Liu H, Ding Y, Yang B, Liu Z, Liu Q, Zhang X. Colorimetric and ultrasensitive detection of H_2O_2 based on Au/Co_3O_4-CeO_x nanocomposites with enhanced peroxidase-like performance. Sens Actuators B Chem. 2018;271:336–45.
28. Ding Y, Yang B, Liu H, Liu Z, Zhang X, Zheng X, et al. FePt-Au ternary metallic nanoparticles with the enhanced peroxidase-like activity for ultrafast colorimetric detection of H_2O_2. Sens Actuators B Chem. 2018;259:775–83.
29. Wu K, Zhao X, Chen M, Zhang H, Liu Z, Zhang X, et al. Synthesis of well-dispersed Fe_3O_4 nanoparticles loaded on montmorillonite and sensitive colorimetric detection of H_2O_2 based on its peroxidase-like activity. New J Chem. 2018;42:9578–87.
30. Zhu X, Chen W, Wu K, Li H, Fu M, Liu Q, et al. A colorimetric sensor of H_2O_2 based on Co_3O_4–montmorillonite nanocomposites with peroxidase activity. New J Chem. 2018;42:1501–9.
31. Houston JB, Kenworthy KE. In vitro-in vivo scaling of CYP kinetic data not consistent with the classical Michaelis-Menten model. Drug Metab Dispos. 2000;28:246–54.
32. Tan H, Ma C, Gao L, Li Q, Song Y, Xu F, et al. Metal-organic framework-derived copper nanoparticle@carbon nanocomposites as peroxidase mimics for colorimetric sensing of ascorbic acid. Chemistry. 2014;20:16377–83.
33. Khataee A, Haddad Irani-Nezhad M, Hassanzadeh J. Improved peroxidase mimetic activity of a mixture of WS_2 nanosheets and silver nanoclusters for chemiluminescent quantification of H_2O_2 and glucose. Microchim Acta. 2018;185:190.
34. Su L, Xiong Y, Yang H, Zhang P, Ye F. Prussian blue nanoparticles encapsulated inside a metal–organic framework via in situ growth as promising peroxidase mimetics for enzyme inhibitor screening. J Mater Chem B. 2016;4:128–34.
35. Zhang XQ, Gong SW, Zhang Y, Yang T, Wang CY, Gu N. Prussian blue modified iron oxide magnetic nanoparticles and their high peroxidase-like activity. J Mater Chem. 2010;20:5110–6.
36. Dong YL, Zhang HG, Rahman ZU, Su L, Chen XJ, Hu J, et al. Graphene oxide-Fe_3O_4 magnetic nanocomposites with peroxidase-like activity for colorimetric detection of glucose. Nanoscale. 2012;4:3969–76.
37. Stratakis M, Garcia H. Catalysis by supported gold nanoparticles: beyond aerobic oxidative processes. Chem Rev. 2012;112:4469–506.
38. Matthey D, Wang JG, Wendt S, Matthiesen J, Schaub R, Laegsgaard E, et al. Enhanced bonding of gold nanoparticles on oxidized TiO_2(110). Science. 2007;315:1692–6.
39. Klyushin AY, Rocha TC, Havecker M, Knop-Gericke A, Schlogl R. A near ambient pressure XPS study of Au oxidation. Phys Chem Chem Phys. 2014;16:7881–6.
40. Huai Q, Zhang B, Sheng F, Tao Z. Raman and ATR infrared studies of the conformation of metallothionein in solution. Spectrosc Lett. 1995;28:829–38.
41. Awotwe-Otoo D, Agarabi C, Keire D, Lee S, Raw A, Yu L, et al. Physicochemical characterization of complex drug substances: evaluation of structural similarities and differences of protamine sulfate from various sources. AAPS J. 2012;14:619–26.
42. Vener MV, Odinokov AV, Wehmeyer C, Sebastiani D. The structure and IR signatures of the arginine-glutamate salt bridge. Insights from the classical MD simulations. J Chem Phys. 2015;142:215106.
43. Zhang JQ, Wang YS, Xue JH, He Y, Yang HX, Liang J, et al. A gold nanoparticles-modified aptamer beacon for urinary adenosine detection based on structure-switching/fluorescence-"turning on" mechanism. J Pharm Biomed Anal. 2012;70:362–8.
44. Xu J, Kong DM. Specific Hg^{2+} quantitation using intramolecular split G-quadruplex DNAzyme. Chin J Anal Chem. 2012;40:347–53.
45. Kong DM, Wang N, Guo XX, Shen HX. 'Turn-on' detection of Hg^{2+} ion using a peroxidase-like split G-quadruplex-hemin DNAzyme. Analyst. 2010;135:545–9.
46. Liu X, Cheng X, Bing T, Fang C, Shangguan D. Visual detection of Hg^{2+} with high selectivity using thymine modified gold nanoparticles. Anal Sci. 2010;26:1169–72.
47. Xu H, Zhu X, Ye H, Yu L, Liu X, Chen G. A simple "molecular beacon"-based fluorescent sensing strategy for sensitive and selective detection of mercury (II). Chem Commun (Camb). 2011;47:12158–60.
48. Ge J, Li XP, Jiang JH, Yu RQ. A highly sensitive label-free sensor for mercury ion (Hg^{2+}) by inhibiting thioflavin T as DNA G-quadruplexes fluorescent inducer. Talanta. 2014;122:85–90.
49. Li Q, Zhou X, Xing D. Rapid and highly sensitive detection of mercury ion (Hg^{2+}) by magnetic beads-based electrochemiluminescence assay. Biosens Bioelectron. 2010;26:859–62.